EurJIC
European Journal of Inorganic Chemistry

Full Paper
doi.org/10.1002/ejic.202000179

Chemistry Europe
European Chemical Societies Publishing

Lithium Stannides

Synthesis, Structural Characterization and Chemical Bonding of $Sr_7Li_6Sn_{12}$ and its Quaternary Derivatives with Eu and Alkaline Earth Metal (Mg, Ca, Ba) Substitutions. A Tale of Seven Li-Containing Stannides and Two Complex Crystal Structures

Hussien H. Osman[a,b] and Svilen Bobev*[b]

Abstract: In this paper, we discuss the synthesis and the structural characterization of the new ternary compound $Sr_7Li_6Sn_{12}$ and its six quaternary derivatives, where alkaline earth metals (Ca, Mg, Ba) and the rare earth metal Eu are substituted, yielding crystalline phases of monoclinic or orthorhombic symmetry. The title compounds were synthesized via high-temperature solid-state reactions of the corresponding elements. The crystal structures were determined by single-crystal X-ray diffraction methods. The $(Sr,Ca)_7Li_6Sn_{12}$ and $Eu_7(Mg,Li)_6Sn_{12}$ phases represent a new structure type (space group *P*2/*m*, No. 10) while $Sr_7Li_6Sn_{12}$ and the rest of the title phases crystallize in the orthorhombic base-centered space group *Cmmm* (No. 65) which is similar to the $Eu_7Li_{8-x}Sn_{10+x}$ ($x \approx 2.0$) phase with the $Ce_7Li_8Ge_{10}$ structure type (Pearson code *oC*50). Careful examination of the resulting structures shows intricate disordering between Li and Sn atoms, which is governed by the total number of valence electrons. The discussion of experimental results is also supported by DFT electronic structure calculations.

Introduction

Polar intermetallics are one of the most structurally diverse classes of solid-state compounds. They are usually made of elements of very different electronegativity, e.g. alkali, alkaline earth, rare earth and early post-transition elements. Such compounds are usually referred to as Zintl phases.[1,2] Due to the large differences in their electronegativities, there is a high degree of polarization of the chemical bonding, akin to that in the molecular substances with polar covalent interactions, the structures are typically rationalized in terms of cations (alkali, alkaline earth, rare earth metals) and anions (the post-transition elements). However, for many lithium-containing compounds, the role of the lightest alkali metal can be viewed as ambivalent. Many recent examples of such phases, including silicides, germanides, stannides, and antimonides have originated from work carried out in our laboratory.[3–13] Of those specifically mentioned here are the rare earth metal–lithium stannides with the general formulas $RE_3Li_{4-x}Sn_{4+x}$ (*RE* = La–Nd, Sm; $x < 0.3$) and $Eu_7Li_{8-x}Sn_{10+x}$ ($x \approx 2.0$),[12] which were an extension of our previous work on structurally related germanide analogs.[5,6,13]

In an earlier publication we discussed the role valence electrons have on the overall structure stability, and this notion was clearly demonstrated in the $Eu_7Li_{8-x}Sn_{10+x}$ ($x \approx 2.0$) system. A severe shortage of valence electrons in the idealized $Eu_7Li_8Sn_{10}$ structure was cited as the reason for the high disordering between Li and Sn atoms (on one position, a nearly 50:50 statistical distribution of Li and Sn).[12] Therefore, the phase $Eu_7Li_{8-x}Sn_{10+x}$ ($x \approx 2.0$) has a very narrow stoichiometry-breadth, as experimentally determined, and the resultant number of valence electrons matches the requirements for optimized Sn–Sn and Li–Sn bonding.

The unusual chemical bonding above piqued our attention, and we sought after more instances of such intricate phenomena. We considered quaternary phases, where multiple cations (of different sizes and electronegativities) were present. It should be noted that very little work has been done on quaternary systems containing lithium and two alkaline-earth metals in combination with tin. Notable exceptions are the compounds $Eu_2Li_xMg_{2-x}Sn_3$ and $Sr_2Li_xMg_{2-x}Sn_3$,[14] which are isotypic with $RE_2Li_2Ge_3$ (*RE* = La–Nd),[5] and crystallize in the orthorhombic space group *Cmcm* (No. 63). They feature infinite chains of Sn, coexisting with isolated Sn_2-dumbbells and Sn atoms.[14] The tin polyanions are separated by Eu/Sr cations, while the Li/Mg atoms are interacting with the Sn atoms in a more covalent manner. This description will be reiterated later on with comparisons to the title phases due to the similarities they share.

In this paper, we report the synthesis and characterization of seven new compounds, whose crystal structures exhibit a great deal of complexity and disordering between Li and Sn atoms. In addition, DFT electronic structure calculations were carried

[a] *Dr. H. H. Osman,*
Chemistry Department, Faculty of Science, Helwan University,
Ain-Helwan, 11795, Cairo, Egypt
E-mail: hokashif@science.helwan.edu.eg
[b] *Dr. H. H. Osman, Prof. S. Bobev*
Department of Chemistry and Biochemistry, University of Delaware,
Newark, Delaware 19716, United States
E-mail: bobev@udel.edu
Supporting information and ORCID(s) from the author(s) for this article are available on the WWW under https://doi.org/10.1002/ejic.202000179.

Full Paper
doi.org/10.1002/ejic.202000179

out for selected model compounds, and discussed in terms of the crystal structure and atomic charges of the composing elements.

Results and Discussion

1. Crystal Structure of Orthorhombic $Sr_7Li_6Sn_{12}$

$Sr_7Li_{8-x}Sn_{10+x}$ (x = 2.07(2)) crystallizes in the orthorhombic space group *Cmmm* (Pearson symbol *oC*50). The phase is isotypic and isoelectronic with the previously reported $Eu_7Li_{8-x}Sn_{10+x}$ (x = 1.99(2)).[12] Its refined composition is $Sr_7Li_{5.93}Sn_{12.07(2)}$ (Table 1), but to be concise, hereafter, this compound will be referred to as $Sr_7Li_6Sn_{12}$. There are four additional phases, synthesized as part of this study that share the same orthorhombic structure–the other being $(Eu,Ba)_7Li_6Sn_{12}$, $(Eu,Ca)_7Li_6Sn_{12}$, $(Sr,Ba)_7Li_6Sn_{12}$ and $Sr_7(Mg,Li)_6Sn_{12}$), all of which were also characterized by single-crystal X-ray diffraction. $Sr_7Li_6Sn_{12}$ was chosen as a representative case for more detailed discussion in the main text, while the structural information for the other isostructural compounds is presented in the Supporting Information section.

Table 1. Data Collection Details and Selected Crystallographic Data for $Sr_7Li_6Sn_{12}$.[a]

chemical formula	$Sr_7Li_{5.93}Sn_{12.07(2)}$
f. wt. (g mol^{-1})	2087.08
a [Å]	7.6166(13)
b [Å]	37.012(6)
c [Å]	4.9139(8)
V [Å^3]	1385.3(4)
$\mu_{MoK\alpha}$ [cm^{-1}]	239.9
$\rho_{calc.}$ (g cm^{-3})	5.00
wR_2 [all data][b]	0.0705
wR_2 [$I > 2\sigma_{(I)}$][b]	0.0655
R_1 [all data][b]	0.0433
R_1 [$I > 2\sigma_{(I)}$][b]	0.0306
$\Delta\rho_{max,min}$ (e Å^{-3})	2.02, −1.84

[a] The structure has the orthorhombic space group *Cmmm* (No. 65) and Z = 2. Data are collected at T = 200 K, Mo-K_α, λ = 0.71073 Å. [b] $R_1 = \Sigma||F_o| - |F_c||/\Sigma|F_o|$; $wR_2 = [\Sigma[w(F_o^2 - F_c^2)^2]/\Sigma[w(F_o^2)^2]]^{1/2}$, and $w = 1/[\sigma^2F_o^2 + (0.03P)^2 + 15.29P]$, where $P = (F_o^2 + 2F_c^2)/3$.

At the outset, we need to mention that the existence of a new Sr–Li–Sn phase was discovered when the exploratory studies of rare-earth metal–lithium stannides with the general formulas $RE_3Li_{4-x}Sn_{4+x}$ (*RE* = La–Nd, Sm; x < 0.3) and $Eu_7Li_{8-x}Sn_{10+x}$ ($x \approx$ 2.0) were ongoing.[12] As part of the work, attempts to make isotypic stannides with the alkaline earth metals Mg, Sr, Ca, Ba (*AE* = alkaline earth metal hereafter) were undertaken. Earlier work suggested the possibility of only being able to make $Sr_7Li_6Sn_{12}$, which is isotypic with the $Eu_7Li_6Sn_{12}$ phase.[12] Crystal quality issues hampered the unequivocal structural elucidation (problems with the collected data resulted in residual peaks near the Sr and Sn atoms) and the question whether or not $Sr_7Li_6Sn_{12}$ is isoelectronic and isostructural with $Eu_7Li_6Sn_{12}$ could not be answered conclusively. Additional tries to improve the crystallinity by starting with different initial compositions and/or varying the heating profiles led to the results recounted in this paper. The previously put forth claims as to the uniqueness of the structure and the validity of the preliminary structural data were further bolstered when quaternary (pseudo-ternary) versions of both $Sr_7Li_6Sn_{12}$ and $Eu_7Li_6Sn_{12}$. These phases were prepared using other *AE* metals to partially substitute Sr and Eu. These studies, which are detailed in the following paragraphs, confirmed that the driving force behind the extensive disordering between Li and Sn atoms must be electronic in nature. Furthermore, the ability to only synthesize compounds based on Sr and Eu (recall that the crystal ionic sizes of Sr^{2+} and Eu^{2+} are very close, ca. 1.32 Å and 1.31 Å, respectively, and sufficiently different from those of Ca^{2+} (1.14 Å) and Ba^{2+} (1.49 Å), respectively[15]) suggested that the geometric factors, i.e., the optimization of the packing efficiency is the reason for the scarcity of other Li–Sn compounds with similar structural characteristics.

Selected crystallographic data for $Sr_7Li_6Sn_{12}$ are shown in Table 1. The structure is fairly complex and it has 10 independent sites in the asymmetric unit cell (Table 2). All atomic positions are fully occupied, except those of the Li atoms, which show unphysical occupation factors exceeding unity. This is especially true on the Li1 site, where the refined electron density is almost a magnitude higher than that, expected for elemental Li. The most likely interpretation of this observation is that Sn atoms are also occupying the same site. The net result is a very high degree of disordering between Li and Sn atoms, accounting for an almost 1:1 statistical mixture on site Li1. Less pronounced, but noticeable Li–Sn disorder also exists on the Li2 site (ca. 40:1 statistical mixture). The occupational Li–Sn disorder on the Li1 position impacts strongly the closest Sn atom, Sn3, which is refined with an enlarged anisotropic displacement without being under-occupied (Table 2). Such disorder has been seen in several previously reported structures such as $Li_{9-x}EuSn_{6+x}$,[14] $RE_3Li_{4-x}Sn_{4+x}$ (*RE* = La–Nd, Sm),[12] $RE_5Li_{2-x}Sn_{7+x}$ (*RE* = Ce, Pr, Nd, Sm),[7] $Li_xT_3Sn_{7-x}$ (*T* = Rh, Ir),[16] $Li_{3-x}Pt_2Sn_{3+x}$,[17] and $Li_{2-x}Pd_2Sn_{5+x}$,[18] all showing that Li atoms are replaced by Sn atoms, or vise versa.

Table 2. Atomic Coordinates and Equivalent Displacements Parameters (U_{eq}[a]) for $Sr_7Li_6Sn_{12}$.

atom	site	x	y	z	U_{eq} [Å^2]
Sr1	4*j*	0	0.1614(1)	1/2	0.020(1)
Sr2	4*j*	0	0.2791(1)	1/2	0.012(1)
Sr3	4*i*	0	0.4447(1)	0	0.013(1)
Sr4	2*a*	0	0	0	0.012(1)
Sn1	8*p*	0.1864(1)	0.2141(1)	0	0.013(1)
Sn2	4*j*	0	0.3757(1)	1/2	0.016(1)
Sn3	4*i*	0	0.0937(1)	0	0.029(1)
Sn4	4*h*	0.3115(1)	0	1/2	0.012(1)
Li1[b]	8*q*	0.1924(12)	0.0764(2)	1/2	0.013(1)
Li2[b]	8*p*	0.3147(10)	0.1406(19)	0	0.013(1)

[a] U_{eq} is defined as 1/3 of the trace of the orthogonalized U_{ij} tensor. [b] Refined mixed occupation of Li and Sn atoms with ratios Li1/Sn = 0.504:0.496(2), Li2/Sn = 0.978:0.022(2).

The structure has already been discussed elsewhere,[12] but it is instructive to briefly recap the basic features again. Several structural representations of the whole unit cell and close-up views of constituting fragments are shown in Figure 1. Viewing the structure approximately down the *c*-axis shows columns of pentagons and hexagons, made up of Sn and Li/Sn atoms. They stacked along the *b*-axis, and the Sr atoms are located within

Full Paper
doi.org/10.1002/ejic.202000179

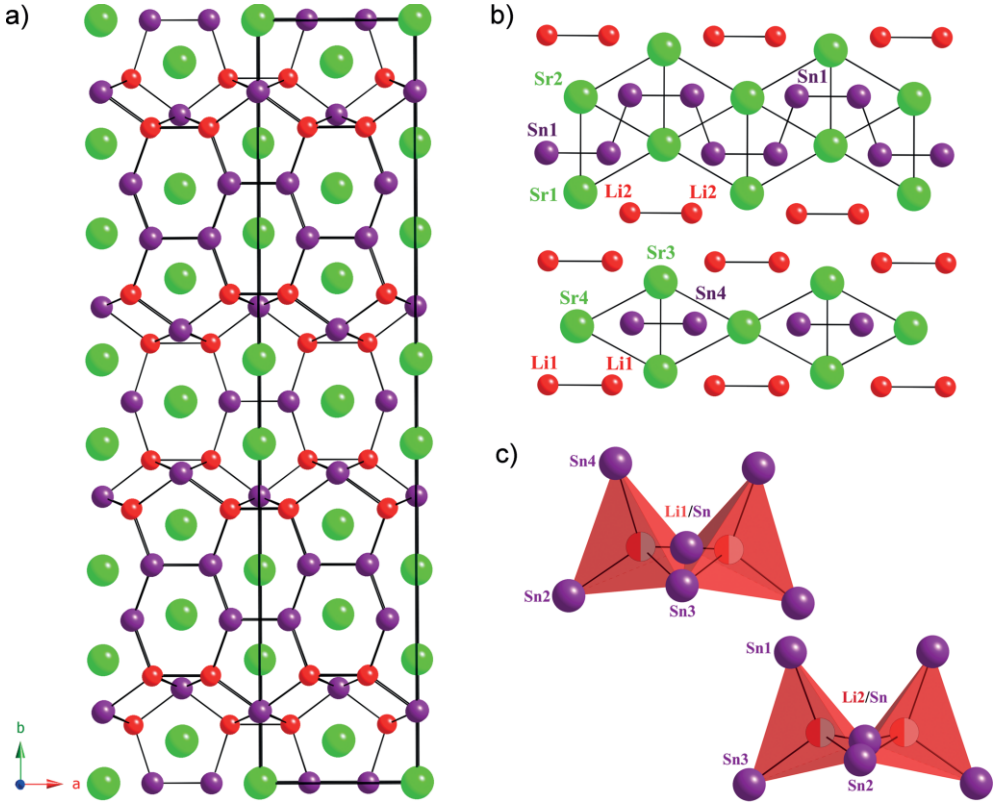

Figure 1. (a) Crystal structure of $Sr_7Li_6Sn_{12}$. In the schematic representation of the orthorhombic structure, the viewing direction is approximately along [001]. Sr atoms are drawn as green spheres; Li and Sn atoms are shown as red and purple spheres, respectively. (b) Close views of the local coordination environments of the *cis*–trans chains and dimers. Further details about the atomic coordinates and the corresponding distances are summarized in Table 2 and Table 3.

them, as depicted in Figure 1a. The structural unit that is perhaps most unusual, is the infinite polyanionic chain, formally assigned as $^1_\infty[Sn_2]^{4-}$, made of alternating cis–trans Sn–Sn pairs (the formal charge assignment is made based on the presumption that the Sn–Sn bonds are single covalent, vide infra). There are also Sn_2-dumbbels, which are in a general sense isolated, as they are surrounded by Li atoms, as shown in the b-panel of Figure 1. However, these are not "pure" Li atoms, as indicated by the refinements (Table 2), which means that 50 % of the time there will be more complex polyanions present–one can envision the existence of another kind of chain made up of Sn_4 tetrahedra sharing corners (or smaller fragments of it), Sn_5-pentagonal units, etc. (Figure S1). Emphasizing the Li substructure and the Li–Sn bonding, the overall $Sr_7Li_6Sn_{12}$ structure can be also viewed as made of $LiSn_4$ tetrahedra, which are connected to each other as depicted in Figure 1c, and joined into the above described tin polyanionic framework, with Sr atoms filling the open space.

Three different types of Sn–Sn distances exist in the $Sr_7Li_6Sn_{12}$ structure. Within the $^1_\infty[Sn_2]$ chains, the cis–bond is 2.839(1) Å long, and the trans–bond is slightly shorter, 2.827(1) Å, respectively (Table 3). Considering the covalent radius of Sn (1.39 Å),[19] the lengths of these bonds are suggestive of the strong covalent character of the interactions. Curiously, both Sn–Sn distances within the chain are shorter than the Sn–Sn bond of the isolated $[Sn_2]$ unit (d_{Sn-Sn} = 2.871(1) Å). These metrics are in good agreement with those for other, previously reported stannides, such as $RELi_{1-x}Sn_2$ ($CeNi_{1-x}Si_2$ structure type),[8] $LiMg(Eu/Sr)_2Sn_3$ ($Ce_2Li_2Ge_3$ structure type),[14] and $LiRh_3Sn_5$ (own structure type),[20] Ca_5Sn_3 (Cr_5B_3 structure type),[21] and $La_{11}Sn_{10}$ ($Ho_{11}Ge_{10}$ structure type).[22] Li–Sn distances are within an agreeable range, which is not surprising given the similarities in the covalent radii of Li and Sn, suggesting covalent character of the interactions as well. Even some of the Sn–Sr distances are within the range of the sum of their single-bonded radii. For example, one can see that the shortest Sn–Sr contact is 3.4355(5) Å (Table 3), which almost matches the sum of the radii of the Sn (1.39 Å) and the Sr (1.95 Å) atoms.[19]

Table 3. Selected interatomic distances [Å] for the $Sr_7Li_6Sn_{12}$ compound.

atom pair	distance
Li1–Li1	2.932(2)
Li1–Sn2	2.935(1)
Li1–Sn3	2.9313(6)
Li1–Sn4	2.972(1)
Li2–Sn1	2.8880(7)
Li2–Sn3	2.9610(7)
Sn1–Sr1 (×4)	3.4425(7)
Sn1–Sr2 (×2)	3.4355(5)
Sn4–Sr3 (×4)	3.5033(7)
Sn4–Sn4	2.871(1)
Sr4–Sn4 (×4)	3.4157(6)
Sr4–Sn3 (×2)	3.4681(9)

Full Paper
doi.org/10.1002/ejic.202000179

2. Crystal Structure of Monoclinic $(Sr,Ca)_7Li_6Sn_{12}$

The Ca-substituted version of $Sr_7Li_6Sn_{12}$ adopts a new type of monoclinic structure, described herein for the first time. It has the monoclinic space group *P*2/*m* (No. 10) and is classified with the Pearson symbol *mP*50. Table 4 summarizes relevant details of the crystallographic work for $(Sr,Ca)_7Li_6Sn_{12}$.

Table 4. Data collection details and selected crystallographic data for $(Sr,Ca)_7Li_6Sn_{12}$.[a]

chemical formula	$Sr_{6.36(2)}Ca_{0.64}Li_{5.98}Sn_{12.02(1)}$
f. wt. (g mol^{-1})	2050.75
a [Å]	15.2337(19)
b [Å]	4.8841(6)
c [Å]	18.827(2)
β (°)	101.688(2)
V [Å^3]	1371.7(3)
$\mu_{MoK\alpha}$ [cm^{-1}]	230.8
$\rho_{calc.}$ (g cm^{-3})	4.97
wR_2 [all data][b]	0.1033
wR_2 [$I > 2\sigma_{(I)}$][b]	0.0905
R_1 [all data][b]	0.0809
R_1 [$I > 2\sigma_{(I)}$][b]	0.0465
$\Delta\rho_{max,min}$ (e Å^{-3})	1.69, −2.36

[a] The structure has the monoclinic space group *P*2/*m* (No. 10) and *Z* = 2. Data are collected at *T* = 200 K, Mo Kα, λ = 0.71073 Å. [b] $R_1 = \Sigma||F_o| - |F_c||/\Sigma|F_o|$; $wR_2 = [\Sigma[w(F_o^2 - F_c^2)^2]/\Sigma[w(F_o^2)^2]]^{1/2}$, and $w = 1/[\sigma^2F_o^2 + (0.0001P)^2 + 7.35P]$, where $P = (F_o^2 + 2F_c^2)/3$.

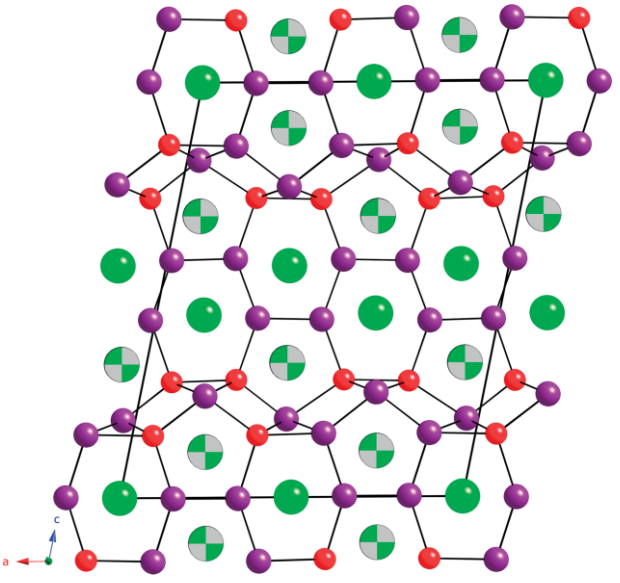

Figure 2. General view of the monoclinic crystal structure of $(Sr,Ca)_7Li_6Sn_{12}$, projected along the *b*-axis. Sr atoms are drawn as green spheres. The mixed occupied Sr/Ca positions are differentiated from those that are refined as 100 % Sr. The Li and Sn atoms are shown as red and purple spheres, respectively. Further details about the atomic coordinates and the corresponding bond lengths are summarized in Table 5 and Table 6.

The structure is schematically represented in Figure 2. As seen from the drawing, $(Sr,Ca)_7Li_6Sn_{12}$ is very closely related to the ternary $Sr_7Li_6Sn_{12}$ phase, and the same attributes described earlier can be identified – the infinite polyanionic cis-trans chains, as well as the tin-dumbbells. Ca atoms replace some of the Sr atoms in random fashion (refined substitution level is ca. 10:1, vide infra). Despite the fact that Ca substitutions occur at only certain Sr positions, there is no observed tendency for Ca and Sr to order crystallographically. In a way, the slight mismatch between the Ca and Sr atoms can be considered as a reason for the distortion of the orthorhombic $Sr_7Li_6Sn_{12}$ structure to the monoclinic $Sr,Ca)_7Li_6Sn_{12}$. $(Sr,Ca)_7Li_6Sn_{12}$ (= $Sr_{6.36(2)}Ca_{0.64}Li_{5.98}Sn_{12.02(1)}$) appears to be a solid solution existing in a narrow range, as all attempts to make the phase with higher or lower Ca content have failed so far. As already alluded to, the existence of this pseudo-ternary phase is governed by the optimization of the packing efficiency (geometric factors) when Sr^{2+} (1.32 Å) is substituted for Ca^{2+} (1.14 Å).[15] Attempting the same type of isovalent substitutions of Sr with either the much smaller Mg, or the much bigger Ba, resulted in the identification of $(Sr,Ba)_7Li_6Sn_{12}$ and $Sr_7(Mg,Li)_6Sn_{12}$ (Tables S1 and S2). On this note, attention has to be brought to the fact that when Mg is introduced, aliovalent substitutions of Li with Mg are likely to occur. This is an indication that the extensive disordering between Li and Sn atoms, which is an electronic effect in nature, allows for an augmented total valence electron count, which can be modulated by varying not only the Li–Sn ratio, but the Li–Mg–Sn ratio as well.

Indeed, the single-crystal data collection details for $Eu_7(Mg,Li)_6Sn_{12}$, presented in Table S5 show this other phase isostructural to $(Sr,Ca)_7Li_6Sn_{12}$ to have a final refined composition of $Eu_7Li_{5.34}Mg_{1.11}Sn_{11.55}$, or, more precisely $Eu_7(Li_{4.89}Mg_{1.11})(Sn_{11.55}Li_{0.45})$. In this structure, Mg atoms cannot replace Eu atoms, but instead they mix with Li atoms, giving rise to a much more complex pattern of the atomic positions (Table S6) compared to the ones listed in Table 5 for $(Sr,Ca)_7Li_6Sn_{12}$.

One distinctive feature of the new monoclinic structure is the local distortions of some the cation coordination polyhedra. Another, is the fact that by lowering the symmetry to monoclinic, a partial Li and Sn ordering is allowed. This is important for understanding the bonding within a whole class of stannides with extensive Li–Sn disorder, specifically $RE_3Li_{4-x}Sn_{4+x}$ (*RE* = La–Nd, Sm; $x < 0.3$),[12] $CaLi_{9-x}Sn_{6+x}$,[14] $Ca_9Li_{6+x}Sn_{13-x}$,[23] as well as $Eu_7Li_{8-x}Sn_{10+x}$ ($x \approx 2.0$). Arguably, the Li and Sn ordering is most relevant to the previously discussed Li1 site in $Sr_7Li_6Sn_{12}$ (Table 2), where the refined model has disordering between Li and Sn atoms in an almost 1:1 statistical distribution. In the paper on $Eu_7Li_{8-x}Sn_{10+x}$ ($x \approx 2.0$), the implications of this 1:1 disorder were discussed, and a possibility of long-range ordered structure with *Pbam* symmetry and doubled unit cell volume was suggested.[12] The reality is that a monoclinic structure with the same cell volume as the base-centered $Sr_7Li_6Sn_{12}$ (in *Cmmm*, vide supra), will also allow for ordering of the 1:1 statistically distributed Li and Sn atoms. The rigorous group-subgroup tree within the Bärnighausen formalism for two structures is presented in the Supporting Information section (Figure S3). Here, in Figure 3, we schematically represent the simpler geometric relationships between the *Cmmm* space group of $Sr_7Li_6Sn_{12}$ (together with its half-volume primitive cell) and the monoclinic *P*2/*m* space group of $(Sr,Ca)_7Li_6Sn_{12}$.

Other attempts to resolve the 1:1 statistical distribution of Li and Sn atoms involved doubling the periodicity along the stacking direction (doubling the *b*-axis in the *Cmmm* structure

Full Paper
doi.org/10.1002/ejic.202000179

Table 5. Atomic coordinates and equivalent displacements parameters (U_{eq}[a] for the $(Sr,Ca)_7Li_6Sn_{12}$ compound.

atom	site	x	y	z	U_{eq} [Å^2]
Sr1[b]	2n	0.0715(1)	1/2	0.3221(1)	0.015(1)
Sr2[b]	2n	0.5897(1)	1/2	0.3237(1)	0.015(1)
Sr3	2n	0.1398(1)	1/2	0.5599(1)	0.013(1)
Sr4	2n	0.3605(1)	1/2	0.4423(1)	0.012(1)
Sr5[b]	2m	0.2781(1)	0	0.1108(1)	0.012(1)
Sr6[b]	2m	0.7769(1)	0	0.1100(1)	0.013(1)
Sr7	1d	1/2	0	0	0.015(1)
Sr8	1a	0	0	0	0.015(1)
Sn1	2m	0.0136(1)	0	0.4283(1)	0.013(1)
Sn2	2m	0.1987(1)	0	0.4245(1)	0.013(1)
Sn3	2m	0.2984(1)	0	0.5686(1)	0.012(1)
Sn4	2m	0.5142(1)	0	0.4277(1)	0.013(1)
Sn5	2n	0.1895(1)	1/2	0.7553(1)	0.014(1)
Sn6	2n	0.3134(1)	1/2	0.2520(1)	0.015(1)
Sn7[c]	2m	0.0349(1)	0	0.1873(1)	0.016(1)
Sn8	2m	0.5594(1)	0	0.1883(1)	0.017(1)
Sn9	2n	0.1566(1)	1/2	0.0024(1)	0.012(1)
Sn10	2n	0.3451(1)	1/2	0.0025(1)	0.012(1)
Sn11[c]	2n	0.1347(1)	1/2	0.1533(1)	0.013(1)
Sn12[c]	2n	0.4423(1)	1/2	0.1535(1)	0.013(1)
Li1[c]	2n	0.0613(5)	1/2	0.8504(5)	0.010(3)
Li2[c]	2n	0.6344(5)	1/2	0.1497(5)	0.008(3)
Li3[c]	2m	0.0847(8)	0	0.7213(7)	0.032(5)
Li4	2m	0.2245(12)	0	0.2788(11)	0.006(4)
Li5	2m	0.2714(12)	0	0.7168(10)	0.004(4)
Li6	2m	0.4146(13)	0	0.2825(13)	0.016(5)

[a] U_{eq} is defined as 1/3 of the trace of the orthogonalized U_{ij} tensor. [b] Refined mixed-occupied positions of Sr and Ca atoms with ratios of Sr1/Ca = 0.82:0.18(1), Sr2/Ca = 0.85:0.15(1), Sr5/Ca = 0.85:0.15(1), and Sr6/Ca = 0.85:0.15(1). [c] Refined mixed-occupied positions with ratios Sn7/Li = 0.964:0.036(4), Sn11/Li = 0.937:0.063(4), Sn12/Li = 0.942:0.058(4), Li1/Sn = 0.938:0.062(4), Li2/Sn = 0.944:0.056(4) and Li3/Sn = 0.956:0.044(4).

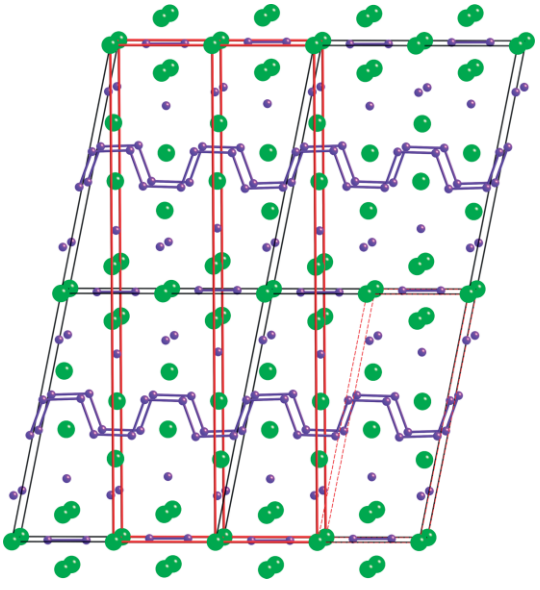

Figure 3. Geometric relationships between the *Cmmm* space group of $Sr_7Li_{8-x}Sn_{10+x}$ ($x \approx 2.0$) (unit cells shown as red outline) and the *P*2/*m* space group of $(Sr,Ca)_7Li_6Sn_{12}$ (unit cells shown in black). The red dashed lines show the primitive cell of the structure with the *Cmmm* space group. Sr atoms are drawn as green, and Sn atoms are shown as purple spheres, respectively.

to ca. 74 Å), as suggested by Xie et al.[24] were not successful. On this note, we must also mention that the compound tentatively assigned in the above-mentioned dissertation as $Sr_{14.5}Li_9Sn_{24}$, is likely the same $Sr_7Li_{8-x}Sn_{10+x}$ ($x \approx 2.0$) phase we are describing here. The compositional difference is, most likely due to the assignment of partially occupied Sn position in the former and the proposed, mixed occupied Sn–Li for the latter (with the nearly equiatomic Li/Sn admixture at Li1 site resolved in the *P*2/*m* space group for the $(Sr,Ca)_7Li_6Sn_{12}$ structure).

With a structural model having ordered Li and Sn atoms, and both in tetrahedral coordination, the structure can be viewed as formed by the said tetrahedral units connected via shared edges and extended as corrugated layers along the *ab*-plane (Figure 4). The space between these tetrahedra is filled with Sr/Ca atoms. The divalent cations are positioned above and below every bend in the chain, in such a way, that each Sn–Sn dimer is encased by four such cations, two above and two below. It should be also pointed out that the "pure" Li positions can be seen playing quite a different role compared to those subjected to considerable mixing with Sn. They are in the plains of the cis–trans chains, and each lithium atom is located adjacent to a tin atom (Figure 5). The overall connectivity resembles that of the hydrogen and carbon atoms in the polyacetylene chains, again attesting to the substantial covalent Li–Sn bond interactions. With this idea in mind, "drawing" bonds between all Sn and Li atoms with $d < 3$ Å shows an array of stacked pentagons and hexagons (Figure 2).

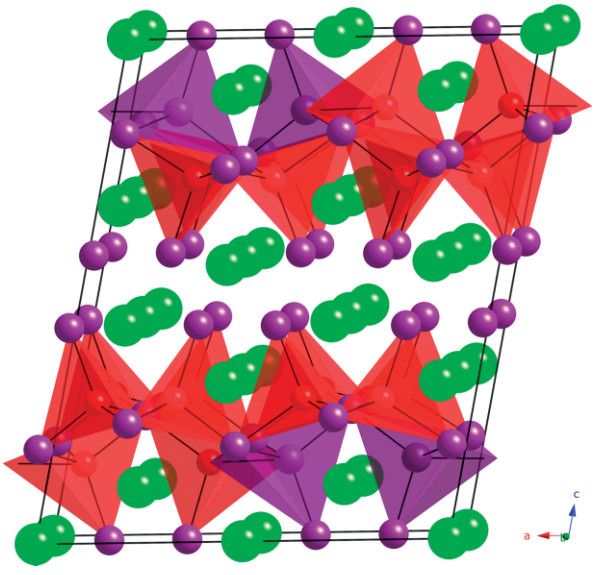

Figure 4. Viewing the crystal structure of the monoclinic $(Sr,Ca)_7Li_6Sn_{12}$ phase as layers of edge-sharing $[LiSn_4]$ and $[SnSn_4]$ tetrahedra. Sn–Sn bonds with the dumbbells and the *cis*–trans chains are omitted for clarity. Further details about the atomic coordinates and the corresponding bond lengths are summarized in Table 5 and Table 6. Sr atoms are drawn as green, and Sn atoms are shown as purple spheres, respectively.

Important interatomic distances for the $(Sr,Ca)_7Li_6Sn_{12}$ are listed in Table 6. As previously mentioned, the distances which we would consider representative of covalent interactions are in quite good agreement with the sum of the corresponding single-bonded radii. Comparing the three specific sets of distances, Li–Li, Li–Sn, and Sn–Sn shows that they are slightly shorter in the $(Sr,Ca)_7Li_6Sn_{12}$ structure. A possible explanation for the

Full Paper
doi.org/10.1002/ejic.202000179

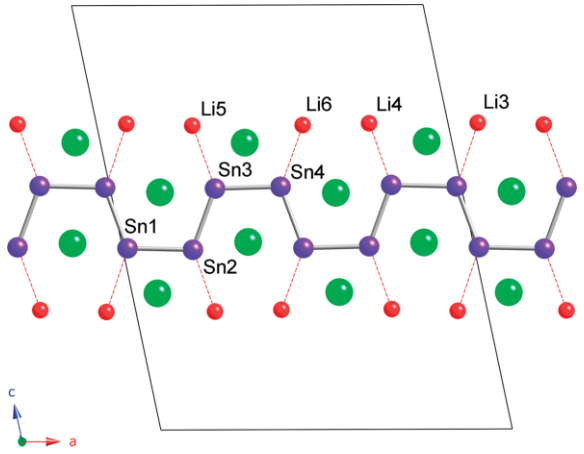

Figure 5. The special positioning of Li atoms around the Sn atoms forming the *cis*–trans chains. Corresponding bond lengths are summarized in Table 6.

slight decrease is that the reduced monoclinic symmetry allows for "relaxation" and less "averaging" of the bonding interactions.

Table 6. Selected interatomic distances [Å] in $(Sr,Ca)_7Li_6Sn_{12}$.

atom pair	distance	atom pair	distance
Sn1–Sn2	2.927(1)	Li2–Sn12 (×2)	2.852(4)
Sn1–Sn4	2.968(1)	Li3–Sn3 (×2)	2.916(7)
Sn1–Sn8 (×2)	3.0127(8)	Li3–Sn7	2.91(1)
Sn6–Sn12 (×2)	3.0170(8)	Li3–Sn8	2.75(2)
Sn7–Sn7	2.815(2)	Li3–Li5	2.86(2)
Sn7–Sn9	2.834(1)	Li5–Sn12	2.82(2)
Sn9–Sn10	2.828(1)	Li6–Sn11	2.85(2)
Sn10–Sn11	2.842(1)	Li4–Li6	2.88(3)
Li1–Sn1	2.973(8)	Sr1–Li3 (×2)	3.393(8)
Li1–Sn2	2.935(8)	Sr2–Sn10 (×2)	3.415(1)
Li1–Sn3	2.903(9)	Sr4–Sn10 (×2)	3.403(1)
Li1–Sn8 (×2)	2.863(4)	Sr4–Li5 (×2)	3.42(1)
Li2–Sn5	2.944(8)	Sr5–Sn5 (×2)	3.465(1)

Similar structural moieties can be recognized in the monoclinic structures of $Eu_7Li_4Bi_6$,[26] $Ba_7Li_{11}Bi_{10}$,[27] as well as in the orthorhombic structures of $Ba_5Cd_2Sb_5F$,[28] and $Eu_5Cd_{4-x}Bi_6$ ($x \approx 1$, frequently referred to as $Eu_{10}Cd_6Bi_{12}$).[29]

3. Electronic Structure of $Sr_7Li_6Sn_{12}$ and $(Sr,Ca)_7Li_6Sn_{12}$

In a previous study, we have discussed the partition of the valence electrons and the electronic structure of the phase $Eu_7Li_{8-x}Sn_{10+x}$ ($x \approx 2$).[12] The same considerations apply to the isoelectronic and isostructural $Sr_7Li_6Sn_{12}$, which was a subject of discussion earlier in this paper. The same electron count can be applied to the monoclinically distorted $(Sr,Ca)_7Li_6Sn_{12}$ too.

Applying the Zintl concept for rationalization of the structures of the title compounds help understanding the necessity for the admixture between Li and Sn atoms at the most basic level. If one considers the final refined formula $Sr_7Li_6Sn_{12}$, and takes into account only the covalent Sn–Sn bonding (Sr and Li atoms are viewed as electron donors), the electron bookkeeping can be done in the following manner: $Sr_7Li_6Sn_{12} = (Sr^{2+})_7(Li^+)_6(2b\text{-}Sn^{2-})_9(4b\text{-}Sn^0)_2(Sn^{4-})(h^+)_2$. The notations 2*b*- and 4*b*- denote Sn atoms with 2 and 4 covalent bonds, while h^+ represents an electron hole. The total valence electron count is 68 valence electrons per formula unit, only 2 electrons short to the optimal 70 electrons/f.u. If admixing between Li and Sn atoms does not exist, in the context of the orthorhombic arrangement and referring specifically to the Li1 site – Table 2, the formula of such hypothetical compound will be $Sr_7Li_8Sn_{10}$. The latter can be broken down to $(Sr^{2+})_7(Li^+)_8(Sn^{4-})_4(1b\text{-}Sn^{3-})_2(2b\text{-}Sn^{2-})_4(h^+)_8$, where 1*b*- refers to the Sn atoms forming dimers with a single covalent bond between them. Correspondingly, the number of available valence electrons for bonding will decrease by 6, and the structure will be electronically destabilized.

Clearly, with so many missing valence electrons, the octets cannot be satisfied. Substituting the electron-richer Sn atom for Li alleviates the shortage and helps bring the overall electron count closer to optimal levels, i.e., the octet rule for such bonding arrangement will hold true.

Let us now move to the theoretical calculations of the electronic structures of the title compounds. In this part, all calculations were performed on three systems: (1) orthorhombic $Sr_7Li_8Sn_{10}$ in *Cmmm* space group (62 e/f.u.), (2) orthorhombic $Sr_7Li_6Sn_{12}$ in *Pbam* space group (68 e/f.u.) and (3) monoclinic $Sr_7Li_6Sn_{12}$ in *P*2/*m* space group (68 e/f.u). Although TB-LMTO-ASA calculations on structure (1) have been done and previously discussed,[12] in this work, all calculations were carried out using the DFT method, as implemented in the VASP program. For practical reasons, all mixed occupied Li and Sn sites were treated as idealized positions occupied by either Li or Sn. The total density of states (TDOS) and the partial contributions of each element (pDOS) of compound (1) are plotted in Figure 6-a. COHP curves for the main three Sn–Sn bonding configurations, e.g. tetrahedral (td), chain (c), and dimer (d), along with the Li–Sn, Sn–Sr, and Li–Li bonds are plotted in Figure 6-b,c. The DOS and pDOS shown in Figure 6-a have similar features to the one, previously reported using the LMTO method for compound (2); $Sr_7Li_6Sn_{12}$ with 68 e/f.u. Two main regions are seen in the DOS plot, one region from the E_F to ca. –3 eV, where the main contribution is from Sr 4*d* and Sn 5*p* orbitals. The other main region is between ca. –4.5 to –9.5 eV, where the contributions are mainly from the Sn 5*s* orbitals. In both regions, weak contributions form Li 2*s* and 2*p* orbitals are also observed. The Fermi level for $Sr_7Li_8Sn_{10}$ corresponds to 62 e/f.u., and it is located near a peak of high DOS, indicating unfavorable electronic structure. The presence of a deep valley in the DOS curve, located ca. 1 eV higher in energy and corresponding to ca. 68 e/f.u., suggests that increasing the number of valence electrons may result in significantly more favorable electronic structure. This confirms the high level of disordering between Li and Sn atoms as a mechanism to alleviate electronic instabilities. As seen in the COHP plots of Figure 6 (b-c), the Sn–Sn bonds at the three conformations; tetrahedral (td), chain (c) and dimer (d), are all in their bonding states. The anti-bonding Sn–Sr states are fully compensated by the Sn–Sn ones. The Li–Sn interactions are mostly optimized at the Fermi level, confirming the covalent nature of the bonding between Li and Sn. Hence the substitution of Li by Sn is expected to enhance the overall stability. The dimerized Sn atoms are showing several

Full Paper
doi.org/10.1002/ejic.202000179

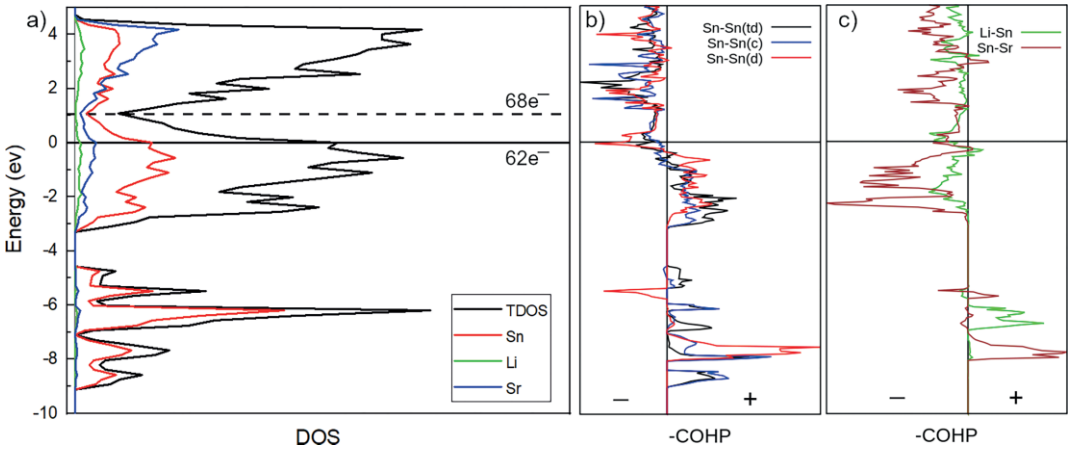

Figure 6. (a) Calculated total DOS diagrams for the orthorhombic $Sr_7Li_8Sn_{10}$ crystal. The Fermi level is set as the energy reference at 0 eV. The partial contribution (pDOS) is attached. (b) COHP curves including the following interactions: the three types of Sn–Sn bonds; tetrahedral (td), chain (c) and dimer (d), Li–Sn and Sn–Sr. Positive and negative signs attached to the COHP curves represent bonding and antibonding states, respectively.

relatively strong peaks in the conduction band above the Fermi level. In the valence band, down to ca. –6 eV, the Sn_2-dimers are in the antibonding states. Similar characteristics of DOS for the homoatomic bonds of many main group element have been reported in previous studies.[25,26,28–32]

Up to this point, the results are in a good agreement with other earlier calculations using more basic computational methodology. The main difference here concerns the Sn–Sr interactions, which appear to have relatively minor contribution. The Sr–Sn interactions are in their (weakly) anti-bonding states at ca. –2.5 eV below the Fermi level, therefore, adding more electrons by virtue of substituting Li atoms with Sn will optimize Sn–Sn and Li–Sn interactions, with minimal effect on Sn–Sr.

The DOS and pDOS of structure (3) are plotted in Figure 7-a. In a comparison to Figure 6, it shows very similar features over the same energy regions, but here the Fermi level is at 68 e/f.u., and it is located right below a local minimum of DOS. In fact, there are two adjacent local minima located above the Fermi level at ca. 0.4 eV. This suggests that increasing the valence electrons to 70 e/f.u. will help to further stabilize the structure. Interestingly, the COHP plot of Figure 7-b,c shows that the Sn–Sr interactions are now well optimized at the Fermi level which proves the idea discussed earlier. In addition, the Sn–Sn and Li–Sn interactions show stronger covalent character than that of the orthorhombic system. It is important to note that the bands seen in Figure 6-b, and attributed to the homoatomic bonding, are not observed here, confirming their absence in (3). The integrated COHP values for selected distances of the two compounds are summarized in Tables S3 and S4.

In terms of Bader charge analysis, the calculated Bader effective charge was obtained for both structures in their ground states. For this purpose, data computed only for structures (2) and (3) were used. The hypothetical structure (1), which is devoid of disorder has a higher total energy was not considered. Selected calculated charges are listed in Table 7. In both systems, Li and Sr atoms have positive charges, which are ca. +0.83 and +1.25, respectively. The Sn atoms have varied negative charges, as expected. In fact, the presence of positive charge less than +1 and +2 on Li and Sr, respectively, indicates the existence of partial covalent interactions between these atoms

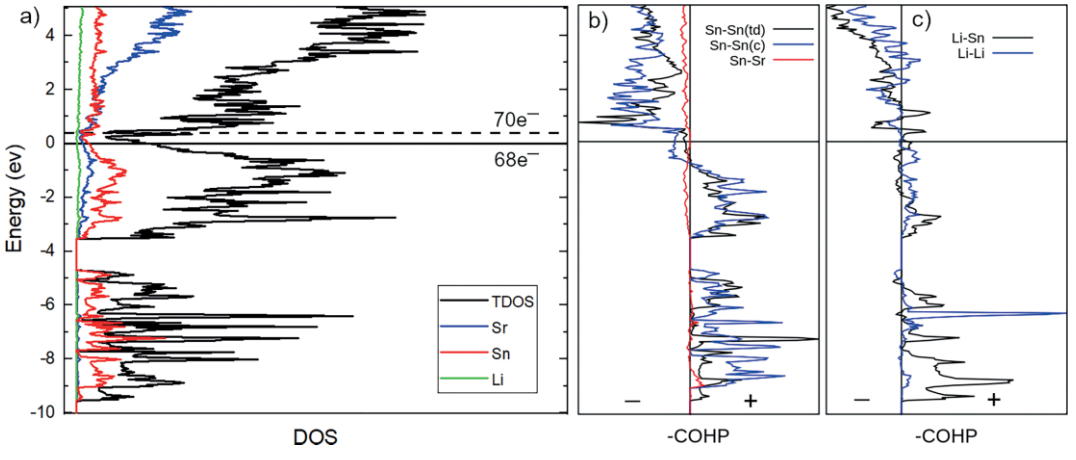

Figure 7. (a) Calculated total DOS diagrams for the monoclinic $Sr_7Li_6Sn_{12}$ crystal in *P2/m* space group. The Fermi level is set as the energy reference at 0 eV. The partial contribution (pDOS) is attached. (b) COHP curves including the following interactions: tetrahedral (td) and chain (c) Sn–Sn interactions, Sn–Sr and Li–Sn. The positive and negative signs attached to the COHP curves represent bonding and antibonding states, respectively.

Full Paper
doi.org/10.1002/ejic.202000179

and the Sn atoms. The negative charge on Sn atoms varies depending on the coordination environment. For instance, the highest negative charge on Sn atoms is ca. −1.8 and −2.2 in structure (2) and (3), respectively. This difference is attributed to the subtle variations in the surrounding of the Sn atoms in question, as schematically in Figure 8.

Table 7. Bader charge average of Sn atoms in the idealized $Sr_7Li_6Sn_{12}$, compared for both *Pbam* and *P*2/*m* space groups.[a]

Pbam	Atom	Sn1	Sn2,Sn3	Sn4	Sn5,Sn6
	Charge	−0.50	−1.05	−1.78	−1.24
P2/m	Atom	Sn1···Sn4	Sn5	Sn6···Sn10	Sn11,Sn12
	Charge	−1.06	−2.24	−1.19	−0.55

[a] The average charge on Li and Sr in both compounds are +0.82 and +1.22, respectively.

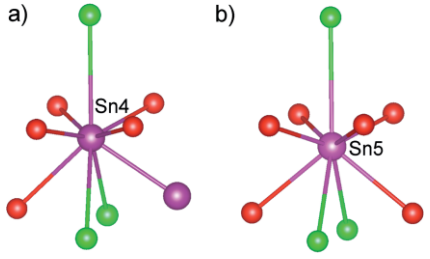

Figure 8. Coordination environment surrounding the Sn atom in (a) compound (2) and (b) compound (3). Sn atoms are depicted in violet, Sr in green and Li in red.

The electron localization function (ELF) analysis of the two structures (1) and (3) is presented in Figure 9. ELF reveals several important bonding features within the system. In general, two main attractors were obtained by ELF analysis: one attractor corresponds to (1) Sn–Sn and (2) Li–Sn bonds as three-dimensional ELF isosurface of value 0.6 around the Sn pentagon connected to Li atoms. The ELF maximum located along the Li–Sn is higher than that of the Sn–Sn reflecting the stronger covalent character of the former. Same information can be extracted from the two-dimensional cross sections of the ELF, as seen in panels b-c. Both cross sections were adjusted on the same ELF range and contour lines interval values. More in-depth analysis shows that the ELF maxima located along the bonding paths of structure (3) have higher values than those of structure (1). This confirms the assumption that increasing the number of valence electrons will help stabilize the system.

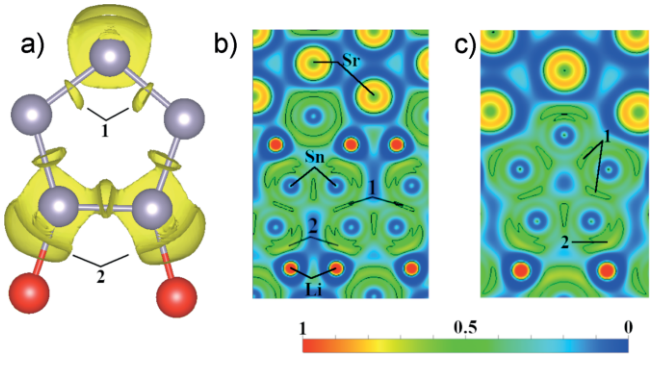

Figure 9. (a) 3D isosurface of ELF for the pentagonal arrangement of tin atoms seen in the monoclinic $Sr_7Li_6Sn_{12}$ crystal structure with *P*2/*m* space group (η = 0.6). Panels (b) and (c) show the cross-sections of the ELF distribution along the [001] plane for the orthorhombic structure (1) (*Cmmm*) and the monoclinic structure (3) (*P*2/*m*), respectively.

Conclusions

This study was focused on the synthesis and the characterization of several new Li-containing compounds, greatly expanding the fundamental knowledge with regards to compounds of the respective elements. The ternary stannide $Sr_7Li_6Sn_{12}$ is the "parent" compound, which was subsequently used as a testbed for isovalent substitutions of Sr with Mg, Ca, Ba and Eu. This work, in turn, led to the successful synthesis of six more quaternary compounds, which can be grouped into two different structure types. One group has an archetype with the general formula $(Ca,Sr)_7Li_6Sn_{12}$, which crystallizes in monoclinic syngony, while the rest are forming orthorhombic crystals with general formulas $(AE,Eu)_7Li_6Sn_{12}$ (*AE* = Ca, Ba), $(Sr,Ba)_7Li_6Sn_{12}$ and $Sr_7(Mg,Li)_6Sn_{12}$. According the structure refinements, alkaline-earth metals like Ca and Ba can replace Sr and Eu while Mg can replace only the Li atoms. Depending on the choice of cations, partial ordering of statistically mixed Li and Sn atoms can be observed, while other structural characteristics are retained.

Experimental Section

All the title phases were prepared and handled in an argon atmosphere using an argon-filled glove box with O_2/H_2O levels below 1 ppm, or under vacuum. All the metals were received and used directly from Alfa with a stated purity of > 99.9 wt.-%. Due to trace amounts of N_2 gas inside the glovebox, the Li rod had to be cleaned carefully with a blade in order to remove the film from Li_3N on the surface. Then, the desired amount of pure Li was cut from it. All the reactions were carried out inside weld-sealed niobium tubes, placed in an evacuated silica jackets. Before their use, the niobium tubes were cleaned with a HNO_3/H_2SO_4/HF mixture, rinsed with distilled water and left overnight in air to dry.

2.1. Synthesis: The title compounds were prepared by direct fusion of the composed elements in Nb tubes. We tried several heating profiles until the best one was obtained. The crystal of $(Sr,Ca)_7Li_{8-x}Sn_{10+x}$ ($x \approx 2.0$) was prepared from reaction of the elements in the molar ration 4:2:7:12 in a total weight of ca. 500 mg. Beyond that, all the other crystals were prepared using the desired stoichiometric ratios. The elemental mixtures were loaded into Nb tubes whose open ends were then closed by arc-welding under argon. The Nb tubes were transferred to fused-silica tubes, which were then flame-sealed under vacuum. The latter step in the preparation was necessary to avoid any contact with air at high temperatures. The mixtures were transferred to a programmable tube furnace and heated to 873 K (20 K/h) for 48 h and then the temperature was raised to 1163 K (25 K/h) dwelled for 72 h. Finally, the reactions were cooled slowly to 373 K with a rate of 5 K/h, and they were removed from the furnace. This method results in silver crystals. The Nb tubes were opened inside the glove box where parts

of the products were ground into powder for the powder diffraction purposes. The powder X-ray diffraction (PXRD) patterns confirmed the air and/or moisture sensitivity of all the title crystals after exposure to air more than 12 h.

2.2. Powder X-ray Diffraction (PXRD)

PXRD patterns were taken on a Rigaku Miniflex diffractometer (filtered Cu Kα radiation, λ = 1.5418 Å), operated inside a nitrogen-filled glovebox so even air-sensitive samples can be handled. Data were collected between 5° and 75° in 2θ with a step size of 0.05° and 2 s/step counting time. The data was analyzed using the JADE 6.5 software package. This analysis provided the phase identification only. In addition, running fresh samples, and samples from the same reaction batch exposed to ambient air (for 12 h) provided evidence that the title compounds are air- and/or moisture-sensitive.

2.3. Single-Crystal X-ray Diffraction (SCXRD): SCXRD measurements were done on a Bruker APEX-II CCD-based diffractometer, equipped with a sealed-tube Mo Kα radiation source (monochromated, λ = 0.71073 Å). Several crystals from each batch were selected under an optical microscope. The selection process was carried out in the glovebox, and the chosen crystals were encased in droplets of Paratone-N oil, deposited on microscope slides. After that, the slides with the crystals were taken out of the glovebox, and individual crystals were picked up with low-background plastic loops. During the data collection, the crystals were subjected to a stream of cold nitrogen gas, necessary to protect them from decomposition/oxidation). Multiple preliminary scans were done for crystals of each batch before the best ones were chosen for full intensity data measurement. The temperature was kept at 200 K throughout the experiment. All the data analysis including the collection, integration and refinement was done using the Bruker-supplied software.[33,34]

For each chosen crystal, measurements were collected with frame width of 0.8° in ω and θ, which allowed to gather a hemisphere of reflections in reciprocal space. Data acquisition rate was 10–15 s/frame. Multi-scan absorption correction was applied using SADABS.[35] The built-in XPREP program[36] was used to analyze the structure factors and to determine the space groups. Crystal structures were solved using the ShelXT program[37] using the intrinsic phasing solution method and were refined using full-matrix least-squares minimization on F^2 with the aid of ShelXL[38] as implemented in Olex2 software package.[39] Refinement parameters were the atomic positions with anisotropic displacements along with the occupancies of Li, Ca and Mg. All the atomic coordinates of the title compounds were standardized using STRUCTURE TIDY.[40]

One important aspect of the crystallographic analysis must be briefly discussed here at the request of a cautious reviewer. As mentioned earlier, over the course of our studies, we became aware of the work by Xie and Nesper,[24] alluding to the formation of a ternary phase, described with the composition $Sr_{14.5}Li_9Sn_{24}$ ($Sr_{7.25}Li_{4.5}Sn_{12}$). Its structure shares many of the same characteristics as $Sr_7Li_{8-x}Sn_{10+x}$ ($x \approx 2.0$) reported in this paper, including the space group. Very likely, it is the same compound, with the apparent compositional difference arising from the structural models: in one case, a mixed-occupied Li-Sn site with ca. 1:1 mixing (this paper); and in the other, a 50 % partially occupied Sn position (ref[24]). Furthermore, Xie's dissertation describes the possibility for doubling the periodicity to resolve structural disorder. This was suggested in both orthorhombic and monoclinic settings, as evidenced from very weak reflections, which were recorded on an image-plate detector. Such long exposure experiments were not done on our CCD-based diffractometer. The currently available to us intensity data were gathered with normal exposure scans, and do not show superstructure reflections. In the future, should crystals of excellent quality become available, pursuing such experiments is called for. Further diffraction studies, inclusive of a total scattering work, will be necessary in order to resolve the discrepancies.

CCDC 1985150 (for $Sr_7Li_6Sn_{12}$), 1985151 (for $(Sr,Ca)_7Li_6Sn_{12}$), 1985152 (for $(Eu,Ba)_7Li_6Sn_{12}$), 1985153 (for $(Eu,Ca)_7Li_6Sn_{12}$), 1985154 (for $(Sr,Ba)_7Li_6Sn_{12}$), 1985155 (for $Sr_7(Li,Mg)_6Sn_{12}$), and 1985156 (for $Eu_7(Li,Mg)_6Sn_{12}$) contain the supplementary crystallographic data for this paper. These data can be obtained free of charge from The Cambridge Crystallographic Data Centre.

2.4. Elemental Micro-analysis: JEOL JSM-6335F scanning electron microscope equipped with an energy-dispersive X-ray (EDX) detector was used to verify the chemical make up of $(Sr,Ca)_7Li_6Sn_{12}$. The amount of lithium could not be ascertained by this method. The EDX was only useful to the point that it verified no unwanted elements heavier then Al are present, and that the elemental Sr/Ca ratio is in agreement with the structure refinements. While it is recognized not as a direct proof, the measured ratio of ca. 10:1, supports the discussed structural model.

2.5. Computational Details: First-principles electronic structure calculations were performed using the projector-augmented wave (PAW) and plane wave basis set scheme under the DFT formalism as implemented in the Vienna ab initio simulation package (VASP).[41–43] Semi-core electrons were included for all the atoms: $4d^{10}5s^25p^2$ of Sn, $4s^24p^65s^2$ of Sr and $1s^22s^1$ of Li. Brillouin-zone integrals were approximated using Gamma-centered Monkhorst–Pack meshes,[44] where the number of subdivisions along each reciprocal lattice vector. Dense *k*-point grids of 3×9×3 and 10×2×14 were used for monoclinic and orthorhombic unit cell, respectively. The wavefunction was expanded in plane waves up to a cut-off energy of 650 eV to ensure convergence of the total energy within 10^{-4} eV per atom. Lattice parameters and atomic positions were optimized at selected volumes and calculations were stopped when the forces on atoms were lower than 10^{-5} eV Å^{-1}. For all the optimized structures, topological analysis of the electron density was carried out using the Bader partitioning method[45] under the Henkelman group code[46] to compute atomic volumes and charges. In addition, the bonding characteristics were studied by the Electron Localization Function analysis.[47,48] The ELF results were visualized with VESTA program.[49] Further chemical-bonding analysis was performed through the crystal orbital Hamilton population (COHP) plots generated by LOBSTER program.[50–53]

Supporting Information Available: Tables with detailed crystallographic information for the other five structures; A figure showing in a schematic way, some of the possible Sn–Sn bonded arrangements that may arise due to the 1:1 mixing; A figure with the crystal structure representations of monoclinic $(Sr,Ca)_7Li_6Sn_{12}$, showing the actual Sn–Sn bonded arrangements that have arisen due to ordering of Li and Sn atoms. A figure with the group–subgroup relationship within the Bärnighausen formalism for the orthorhombic structures of $Sr_7Li_6Sn_{12}$ and the monoclinic structure $(Sr,Ca)_7Li_6Sn_{12}$ is also included.

Acknowledgments

This work was supported by the US National Science Foundation, grant DMR-1709813. The authors thank Mr. Jordan Sinclair for proof-reading the manuscript.

Keywords: Crystal Structure · Lithium · Solid-State Synthesis · Stannide · Zintl phases

[1] E. Zint–6l, *Angew. Chem.* **1939**, *52*, 1.
[2] *Chemistry, Structure, and Bonding of Zintl Phases and Ions* (Ed.: S. M. Kauzlarich), Wiley-VCH, New York. **1996**. ISBN 1–56081–900–6.
[3] T.-S. You, S. Bobev, *J. Solid State Chem.* **2010**, *183*, 2895–2902.
[4] S. Bobev, T.-S. You, N.-T. Suen, S. Saha, R. Greene, J. Paglione, *Inorg. Chem.* **2011**, *51*, 620–628.
[5] S.-P. Guo, T.-S. You, S. Bobev, *Inorg. Chem.* **2012**, *51*, 3119–3129.
[6] S.-P. Guo, T.-S. You, Y.-H. Jung, S. Bobev, *Inorg. Chem.* **2012**, *51*, 6821–6829.
[7] J. P. A. Makongo, S. Bobev, *Acta Crystallogr., Sect. C* **2014**, *70*, 2–6.
[8] J. P. A. Makongo, N.-T. Suen, S.-P. Guo, S. Saha, R. Greene, J. Paglione, S. Bobev, *J. Solid State Chem.* **2014**, *211*, 95–105.
[9] J. P. A. Makongo, T.-S. You, H. He, N.-T. Suen, S. Bobev, *Eur. J. Inorg. Chem.* **2014**, *2014*, 5113–5124.
[10] M. C. Schäfer, N.-T. Suen, M. Raglione, S. Bobev, *J. Solid State Chem.* **2014**, *210*, 85–95.
[11] R. Zhao, S. Bobev, L. Krishna, T. Yang, J. M. Weller, H. Jing, C. K. Chan, *ACS Appl. Mater. Interfaces* **2017**, *9*, 41246–41257.
[12] N.-T. Suen, S.-P. Guo, J. Hoos, S. Bobev, *Inorg. Chem.* **2018**, *57*, 5632–5641.
[13] N.-T. Suen, T.-S. You, S. Bobev, *Acta Crystallogr., Sect. C* **2013**, *69*, 1–4.
[14] I. Todorov, S. C. Sevov, *Inorg. Chem.* **2005**, *44*, 5361–5369.
[15] R. D. Shannon, *Acta Crystallogr., Sect. A* **1976**, *32*, 751–767.
[16] P. Sreeraj, D. Kurowski, R.-D. Hoffmann, Z. Wu, R. Pöttgen, *J. Solid State Chem.* **2005**, *178*, 3420–3425.
[17] R.-D. Hoffmann, Z. Wu, R. Pöttgen, *Eur. J. Inorg. Chem.* **2003**, 3425–3431.
[18] P. Sreeraj, R.-D. Hoffmann, Z. Wu, R. Pöttgen, U. Häussermann, *ChemInform.* **2005**, 36.
[19] B. Cordero, V. Gómez, A. E. Platero-Prats, M. Revés, J. Echeverría, E. Cremades, F. Barragán, S. Alvarez, *Dalton Trans.* **2008**, 2832–2838.
[20] P. Sreeraj, D. Johrendt, H. Müller, R.-D. Hoffmann, Z. Wu, R. Pöttgen, *Z. Naturforsch. B* **2005**, *60*, 933–939.
[21] E. A. Leon-Escamilla, J. D. Corbett, *J. Solid State Chem.* **2001**, *159*, 149–162.
[22] I. Dürr, C. Röhr, *Z. Anorg. Allg. Chem.* **2012**, *638*, 163–176.
[23] A. Ovchinnikov, S. Bobev, *Dalton Trans.* **2019**, *48*, 14398–14407.
[24] Q. Xie, *Syntheses, Structures, and Properties of Multinary Zintl Phases and their Decomposition Reactions*, ETH Zurich, Dissertation No. 15626.
[25] M. C. Schäfer, N.-T. Suen, S. Bobev, *Dalton Trans.* **2014**, *43*, 16889–16901.
[26] D. O. Ojwang, S. Bobev, *Inorganics* **2018**, *6*, 109–126.
[27] B. Saparov, S. Bobev, *Dalton Trans.* **2010**, *39*, 11335–11343.
[28] S.-Q. Xia, S. Bobev, *Chem. Asian J.* **2007**, *2*, 619–624.
[29] A. B. Childs, S. Baranets, S. Bobev, *J. Solid State Chem.* **2019**, *278*, 120889–120898.
[30] S. Baranets, S. Bobev, *Inorg. Chem.* **2019**, *58*, 8506–8516.
[31] S.-Q. Xia, S. Bobev, *J. Comput. Chem.* **2008**, *29*, 2125–2133.
[32] J. Xu, H. Kleinke, *J. Comput. Chem.* **2008**, *29*, 2134–2143.
[33] *SMART NT*; Bruker Analytical X-ray Systems, Inc.: Madison, WI, (**2003**).
[34] *SAINT NT*; Bruker Analytical X-ray Systems, Inc.: Madison, WI, (**2003**).
[35] *SADABS*; Bruker Analytical X-ray Systems Inc.: Madison, WI, (**2014**).
[36] *XPREP*; Bruker Analytical X-ray Systems Inc.: Madison, WI, (**2014**).
[37] G. M. Sheldrick, *Acta Crystallogr., Sect. A* **2015**, *71*, 3–8.
[38] G. M. Sheldrick, *Acta Crystallogr., Sect. C* **2015**, *71*, 3–8.
[39] O. V. Dolomanov, L. J. Bourhis, R. J. Gildea, J. A. K. Howard, H. Puschmann, *J. Appl. Crystallogr.* **2009**, *42*, 339–341.
[40] L. M. Gelato, E. Parthé, *J. Appl. Crystallogr.* **1987**, *20*, 139–143.
[41] P. E. Blöchl, *Phys. Rev. B* **1994**, *50*, 17953–17979.
[42] G. Kresse, J. Furthmüller, *Phys. Rev. B* **1996**, *54*, 11169–11186.
[43] G. Kresse, D. Joubert, *Phys. Rev. B* **1999**, *59*, 1758–1775.
[44] H. J. Monkhorst, J. D. Pack, *Phys. Rev. B* **1976**, *13*, 5188–5192.
[45] R. F. W. Bader, in *Atoms in Molecules: A Quantum Theory* (Eds.: J. Halpern, M. L. H. Green), The International Series of Monographs of Chemistry, Clarendon Press, Oxford, UK, **1990**.
[46] W. Tang, E. Sanville, G. Henkelman, *J. Phys. Condens. Matter* **2009**, *21*, 084204.
[47] A. Savin, R. Nesper, S. Wengert, T. F. Faessler, *Angew. Chem. Int. Ed. Engl.* **1997**, *36*, 1808–1832; *Angew. Chem.* **1997**, *109*, 1892.
[48] A. Savin, *THEOCHEM* **2005**, *727*, 127–131.
[49] K. Momma, F. Izumi, *J. Appl. Crystallogr.* **2011**, *44*, 1272–1276.
[50] V. L. Deringer, A. L. Tchougréeff, R. Dronskowski, *J. Phys. Chem. A* **2011**, *115*, 5461–5466.
[51] R. Dronskowski, P. E. Blöchl, *J. Phys. Chem.* **1993**, *97*, 8617–8624.
[52] S. Maintz, V. L. Deringer, A. L. Tchougréeff, R. Dronskowski, *J. Comput. Chem.* **2013**, *34*, 2557–2567.
[53] S. Maintz, V. L. Deringer, A. L. Tchougréeff, R. Dronskowski, *J. Comput. Chem.* **2016**, *37*, 1030–1035.

Received: February 21, 2020